Measurement of the form factors in the decay $D^+ \to \omega e^+ \nu_e$ and search for the decay $D^+ \to \phi e^+ \nu_e$

M. Ablikim,[1] M. N. Achasov,[9,f] X. C. Ai,[1] O. Albayrak,[5] M. Albrecht,[4] D. J. Ambrose,[44] A. Amoroso,[49a,49c] F. F. An,[1] Q. An,[46,a] J. Z. Bai,[1] R. Baldini Ferroli,[20a] Y. Ban,[31] D. W. Bennett,[19] J. V. Bennett,[5] M. Bertani,[20a] D. Bettoni,[21a] J. M. Bian,[43] F. Bianchi,[49a,49c] E. Boger,[23,d] I. Boyko,[23] R. A. Briere,[5] H. Cai,[51] X. Cai,[1,a] O. Cakir,[40a,b] A. Calcaterra,[20a] G. F. Cao,[1] S. A. Cetin,[40b] J. F. Chang,[1,a] G. Chelkov,[23,d,e] G. Chen,[1] H. S. Chen,[1] H. Y. Chen,[2] J. C. Chen,[1] M. L. Chen,[1,a] S. J. Chen,[29] X. Chen,[1,a] X. R. Chen,[26] Y. B. Chen,[1,a] H. P. Cheng,[17] X. K. Chu,[31] G. Cibinetto,[21a] H. L. Dai,[1,a] J. P. Dai,[34] A. Dbeyssi,[14] D. Dedovich,[23] Z. Y. Deng,[1] A. Denig,[22] I. Denysenko,[23] M. Destefanis,[49a,49c] F. De Mori,[49a,49c] Y. Ding,[27] C. Dong,[30] J. Dong,[1,a] L. Y. Dong,[1] M. Y. Dong,[1,a] S. X. Du,[53] P. F. Duan,[1] E. E. Eren,[40b] J. Z. Fan,[39] J. Fang,[1,a] S. S. Fang,[1] X. Fang,[46,a] Y. Fang,[1] L. Fava,[49b,49c] F. Feldbauer,[22] G. Felici,[20a] C. Q. Feng,[46,a] E. Fioravanti,[21a] M. Fritsch,[14,22] C. D. Fu,[1] Q. Gao,[1] X. Y. Gao,[2] Y. Gao,[39] Z. Gao,[46,a] I. Garzia,[21a] K. Goetzen,[10] W. X. Gong,[1,a] W. Gradl,[22] M. Greco,[49a,49c] M. H. Gu,[1,a] Y. T. Gu,[12] Y. H. Guan,[1] A. Q. Guo,[1] L. B. Guo,[28] Y. Guo,[1] Y. P. Guo,[22] Z. Haddadi,[25] A. Hafner,[22] S. Han,[51] X. Q. Hao,[15] F. A. Harris,[42] K. L. He,[1] X. Q. He,[45] T. Held,[4] Y. K. Heng,[1,a] Z. L. Hou,[1] C. Hu,[28] H. M. Hu,[1] J. F. Hu,[49a,49c] T. Hu,[1,a] Y. Hu,[1] G. M. Huang,[6] G. S. Huang,[46,a] J. S. Huang,[15] X. T. Huang,[33] Y. Huang,[29] T. Hussain,[48] Q. Ji,[1] Q. P. Ji,[30] X. B. Ji,[1] X. L. Ji,[1,a] L. W. Jiang,[51] X. S. Jiang,[1,a] X. Y. Jiang,[30] J. B. Jiao,[33] Z. Jiao,[17] D. P. Jin,[1,a] S. Jin,[1] T. Johansson,[50] A. Julin,[43] N. Kalantar-Nayestanaki,[25] X. L. Kang,[1] X. S. Kang,[30] M. Kavatsyuk,[25] B. C. Ke,[5] P. Kiese,[22] R. Kliemt,[14] B. Kloss,[22] O. B. Kolcu,[40b,i] B. Kopf,[4] M. Kornicer,[42] W. Kühn,[24] A. Kupsc,[50] J. S. Lange,[24] M. Lara,[19] P. Larin,[14] C. Leng,[49c] C. Li,[50] Cheng Li,[46,a] D. M. Li,[53] F. Li,[1,a] F. Y. Li,[31] G. Li,[1] H. B. Li,[1] J. C. Li,[1] Jin Li,[32] K. Li,[33] K. Li,[13] Lei Li,[3] P. R. Li,[41] T. Li,[33] W. D. Li,[1] W. G. Li,[1] X. L. Li,[33] X. M. Li,[12] X. N. Li,[1,a] X. Q. Li,[30] Z. B. Li,[38] H. Liang,[46,a] Y. F. Liang,[36] Y. T. Liang,[24] G. R. Liao,[11] D. X. Lin,[14] B. J. Liu,[1] C. X. Liu,[1] F. H. Liu,[35] Fang Liu,[1] Feng Liu,[6] H. B. Liu,[12] H. H. Liu,[16] H. H. Liu,[1] H. M. Liu,[1] J. Liu,[1] J. B. Liu,[46,a] J. P. Liu,[51] J. Y. Liu,[1] K. Liu,[39] K. Y. Liu,[27] L. D. Liu,[31] P. L. Liu,[1,a] Q. Liu,[41] S. B. Liu,[46,a] X. Liu,[26] Y. B. Liu,[30] Z. A. Liu,[1,a] Zhiqing Liu,[22] H. Loehner,[25] X. C. Lou,[1,a,h] H. J. Lu,[17] J. G. Lu,[1,a] Y. Lu,[1] Y. P. Lu,[1,a] C. L. Luo,[28] M. X. Luo,[52] T. Luo,[42] X. L. Luo,[1,a] X. R. Lyu,[41] F. C. Ma,[27] H. L. Ma,[1] L. L. Ma,[33] Q. M. Ma,[1] T. Ma,[1] X. N. Ma,[30] X. Y. Ma,[1,a] F. E. Maas,[14] M. Maggiora,[49a,49c] Y. J. Mao,[31] Z. P. Mao,[1] S. Marcello,[49a,49c] J. G. Messchendorp,[25] J. Min,[1,a] R. E. Mitchell,[19] X. H. Mo,[1,a] Y. J. Mo,[6] C. Morales Morales,[14] K. Moriya,[19] N. Yu. Muchnoi,[9,f] H. Muramatsu,[43] Y. Nefedov,[23] F. Nerling,[14] I. B. Nikolaev,[9,f] Z. Ning,[1,a] S. Nisar,[8] S. L. Niu,[1,a] X. Y. Niu,[1] S. L. Olsen,[32] Q. Ouyang,[1,a] S. Pacetti,[20b] P. Patteri,[20a] M. Pelizaeus,[4] H. P. Peng,[46,a] K. Peters,[10] J. Pettersson,[50] J. L. Ping,[28] R. G. Ping,[1] R. Poling,[43] V. Prasad,[1] M. Qi,[29] S. Qian,[1,a] C. F. Qiao,[41] L. Q. Qin,[33] N. Qin,[51] X. S. Qin,[1] Z. H. Qin,[1,a] J. F. Qiu,[1] K. H. Rashid,[48] C. F. Redmer,[22] M. Ripka,[22] G. Rong,[1] Ch. Rosner,[14] X. D. Ruan,[12] V. Santoro,[21a] A. Sarantsev,[23,g] M. Savrié,[21b] K. Schoenning,[50] S. Schumann,[22] W. Shan,[31] M. Shao,[46,a] C. P. Shen,[2] P. X. Shen,[30] X. Y. Shen,[1] H. Y. Sheng,[1] W. M. Song,[1] X. Y. Song,[1] S. Sosio,[49a,49c] S. Spataro,[49a,49c] G. X. Sun,[1] J. F. Sun,[15] S. S. Sun,[1] Y. J. Sun,[46,a] Y. Z. Sun,[1] Z. J. Sun,[1,a] Z. T. Sun,[19] C. J. Tang,[36] X. Tang,[1] I. Tapan,[40c] E. H. Thorndike,[44] M. Tiemens,[25] M. Ullrich,[24] I. Uman,[40b] G. S. Varner,[42] B. Wang,[30] D. Wang,[31] D. Y. Wang,[31] K. Wang,[1,a] L. L. Wang,[1] L. S. Wang,[1] M. Wang,[33] P. Wang,[1] P. L. Wang,[1] S. G. Wang,[31] W. Wang,[1,a] X. F. Wang,[39] Y. D. Wang,[14] Y. F. Wang,[1,a] Y. Q. Wang,[22] Z. Wang,[1,a] Z. G. Wang,[1,a] Z. H. Wang,[46,a] Z. Y. Wang,[1] T. Weber,[22] D. H. Wei,[11] J. B. Wei,[31] P. Weidenkaff,[22] S. P. Wen,[1] U. Wiedner,[4] M. Wolke,[50] L. H. Wu,[1] Z. Wu,[1,a] L. G. Xia,[39] Y. Xia,[18] D. Xiao,[1] H. Xiao,[47] Z. J. Xiao,[28] Y. G. Xie,[1,a] Q. L. Xiu,[1,a] G. F. Xu,[1] L. Xu,[1] Q. J. Xu,[13] X. P. Xu,[37] L. Yan,[46,a] W. B. Yan,[46,a] W. C. Yan,[46,a] Y. H. Yan,[18] H. J. Yang,[34] H. X. Yang,[1] L. Yang,[51] Y. Yang,[6] Y. X. Yang,[11] M. Ye,[1,a] M. H. Ye,[7] J. H. Yin,[1] B. X. Yu,[1,a] C. X. Yu,[30] J. S. Yu,[26] C. Z. Yuan,[1] W. L. Yuan,[29] Y. Yuan,[1] A. Yuncu,[40b,c] A. A. Zafar,[48] A. Zallo,[20a] Y. Zeng,[18] B. X. Zhang,[1] B. Y. Zhang,[1,a] C. Zhang,[29] C. C. Zhang,[1] D. H. Zhang,[1] H. H. Zhang,[38] H. Y. Zhang,[1,a] J. J. Zhang,[1] J. L. Zhang,[1] J. Q. Zhang,[1] J. W. Zhang,[1,a] J. Y. Zhang,[1] J. Z. Zhang,[1] K. Zhang,[1] L. Zhang,[1] X. Y. Zhang,[33] Y. Zhang,[1] Y. N. Zhang,[41] Y. H. Zhang,[1,a] Y. T. Zhang,[46,a] Yu Zhang,[41] Z. H. Zhang,[6] Z. P. Zhang,[46] Z. Y. Zhang,[51] G. Zhao,[1] J. W. Zhao,[1,a] J. Y. Zhao,[1] J. Z. Zhao,[1,a] Lei Zhao,[46,a] Ling Zhao,[1] M. G. Zhao,[30] Q. Zhao,[1] Q. W. Zhao,[1] S. J. Zhao,[53] T. C. Zhao,[1] X. H. Zhao,[29] Y. B. Zhao,[1,a] Z. G. Zhao,[46,a] A. Zhemchugov,[23,d] B. Zheng,[47] J. P. Zheng,[1,a] W. J. Zheng,[33] Y. H. Zheng,[41] B. Zhong,[28] L. Zhou,[1,a] X. Zhou,[51] X. K. Zhou,[46,a] X. R. Zhou,[46,a] X. Y. Zhou,[1] K. Zhu,[1] K. J. Zhu,[1,a] S. Zhu,[1] S. H. Zhu,[45] X. L. Zhu,[39] Y. C. Zhu,[46,a] Y. S. Zhu,[1] Z. A. Zhu,[1] J. Zhuang,[1,a] L. Zotti,[49a,49c] B. S. Zou,[1] and J. H. Zou[1]

(BESIII Collaboration)

[1]Institute of High Energy Physics, Beijing 100049, People's Republic of China
[2]Beihang University, Beijing 100191, People's Republic of China
[3]Beijing Institute of Petrochemical Technology, Beijing 102617, People's Republic of China
[4]Bochum Ruhr-University, D-44780 Bochum, Germany
[5]Carnegie Mellon University, Pittsburgh, Pennsylvania 15213, USA
[6]Central China Normal University, Wuhan 430079, People's Republic of China
[7]China Center of Advanced Science and Technology, Beijing 100190, People's Republic of China
[8]COMSATS Institute of Information Technology, Lahore, Defence Road, Off Raiwind Road,
54000 Lahore, Pakistan
[9]G.I. Budker Institute of Nuclear Physics SB RAS (BINP), Novosibirsk 630090, Russia
[10]GSI Helmholtzcentre for Heavy Ion Research GmbH, D-64291 Darmstadt, Germany
[11]Guangxi Normal University, Guilin 541004, People's Republic of China
[12]GuangXi University, Nanning 530004, People's Republic of China
[13]Hangzhou Normal University, Hangzhou 310036, People's Republic of China
[14]Helmholtz Institute Mainz, Johann-Joachim-Becher-Weg 45, D-55099 Mainz, Germany
[15]Henan Normal University, Xinxiang 453007, People's Republic of China
[16]Henan University of Science and Technology, Luoyang 471003, People's Republic of China
[17]Huangshan College, Huangshan 245000, People's Republic of China
[18]Hunan University, Changsha 410082, People's Republic of China
[19]Indiana University, Bloomington, Indiana 47405, USA
[20a]INFN Laboratori Nazionali di Frascati, I-00044 Frascati, Italy
[20b]INFN and University of Perugia, I-06100 Perugia, Italy
[21a]INFN Sezione di Ferrara, I-44122 Ferrara, Italy
[21b]University of Ferrara, I-44122 Ferrara, Italy
[22]Johannes Gutenberg University of Mainz, Johann-Joachim-Becher-Weg 45,
D-55099 Mainz, Germany
[23]Joint Institute for Nuclear Research, 141980 Dubna, Moscow region, Russia
[24]Justus Liebig University Giessen, II. Physikalisches Institut, Heinrich-Buff-Ring 16,
D-35392 Giessen, Germany
[25]KVI-CART, University of Groningen, NL-9747 AA Groningen, Netherlands
[26]Lanzhou University, Lanzhou 730000, People's Republic of China
[27]Liaoning University, Shenyang 110036, People's Republic of China
[28]Nanjing Normal University, Nanjing 210023, People's Republic of China
[29]Nanjing University, Nanjing 210093, People's Republic of China
[30]Nankai University, Tianjin 300071, People's Republic of China
[31]Peking University, Beijing 100871, People's Republic of China
[32]Seoul National University, Seoul 151-747, Korea
[33]Shandong University, Jinan 250100, People's Republic of China
[34]Shanghai Jiao Tong University, Shanghai 200240, People's Republic of China
[35]Shanxi University, Taiyuan 030006, People's Republic of China
[36]Sichuan University, Chengdu 610064, People's Republic of China
[37]Soochow University, Suzhou 215006, People's Republic of China
[38]Sun Yat-Sen University, Guangzhou 510275, People's Republic of China
[39]Tsinghua University, Beijing 100084, People's Republic of China
[40a]Istanbul Aydin University, 34295 Sefakoy, Istanbul, Turkey
[40b]Dogus University, 34722 Istanbul, Turkey
[40c]Uludag University, 16059 Bursa, Turkey
[41]University of Chinese Academy of Sciences, Beijing 100049, People's Republic of China
[42]University of Hawaii, Honolulu, Hawaii 96822, USA
[43]University of Minnesota, Minneapolis, Minnesota 55455, USA
[44]University of Rochester, Rochester, New York 14627, USA
[45]University of Science and Technology Liaoning, Anshan 114051, People's Republic of China
[46]University of Science and Technology of China, Hefei 230026, People's Republic of China
[47]University of South China, Hengyang 421001, People's Republic of China
[48]University of the Punjab, Lahore 54590, Pakistan
[49a]University of Turin, I-10125 Turin, Italy
[49b]University of Eastern Piedmont, I-15121 Alessandria, Italy
[49c]INFN, I-10125 Turin, Italy
[50]Uppsala University, Box 516, SE-75120 Uppsala, Sweden
[51]Wuhan University, Wuhan 430072, People's Republic of China

^{52}*Zhejiang University, Hangzhou 310027, People's Republic of China*
^{53}*Zhengzhou University, Zhengzhou 450001, People's Republic of China*

Using 2.92 fb^{-1} of electron-positron annihilation data collected at a center-of-mass energy of $\sqrt{s} = 3.773$ GeV with the BESIII detector, we present an improved measurement of the branching fraction $\mathcal{B}(D^+ \to \omega e^+ \nu_e) = (1.63 \pm 0.11 \pm 0.08) \times 10^{-3}$. The parameters defining the corresponding hadronic form factor ratios at zero momentum transfer are determined for the first time; we measure them to be $r_V = 1.24 \pm 0.09 \pm 0.06$ and $r_2 = 1.06 \pm 0.15 \pm 0.05$. The first and second uncertainties are statistical and systematic, respectively. We also search for the decay $D^+ \to \phi e^+ \nu_e$. An improved upper limit $\mathcal{B}(D^+ \to \phi e^+ \nu_e) < 1.3 \times 10^{-5}$ is set at 90% confidence level.

Charm semileptonic decays have been studied in detail because they provide essential inputs of the magnitudes of the Cabibbo-Kobayashi-Maskawa (CKM) elements $|V_{cd}|$ and $|V_{cs}|$ [1,2], and a stringent test of the strong interaction effects in the decay amplitude. These effects of the strong interaction in the hadronic current are parametrized by form factors that are calculable, for example, by lattice QCD and QCD sum rules. The couplings $|V_{cs}|$ and $|V_{cd}|$ are tightly constrained by the unitarity of the CKM matrix. Therefore, measurements of charm semileptonic decay rates and form factors rigorously test theoretical predictions. Both high statistics and rare modes should be studied for a comprehensive understanding of charm semileptonic decays.

For $D \to V\ell\nu$ transitions (where V refers to a vector meson), the form factors have been studied in the decays $D^+ \to \bar{K}^{*0}e^+\nu_e$ [3] and $D^+ \to \rho^0 e^+\nu_e$ [4]. The decay $D^+ \to \omega e^+\nu_e$ was first observed by the CLEO-c experiment, while the corresponding form factors have not yet been measured due to limited statistics [4]. The transition rate of the decay $D^+ \to \omega e^+\nu_e$ depends on the charm-to-down-quark coupling $|V_{cd}|$, which is precisely known from unitarity of the CKM matrix. Neglecting the lepton mass, three dominant form factors contribute to the decay rate: two axial (A_1, A_2) and one vector (V) form factor, which are functions of the square of the invariant mass of the lepton-neutrino system q^2.

The decay $D^+ \to \phi e^+\nu_e$ has not yet been observed. The most recent experimental search was performed by the CLEO collaboration in 2011 with a sample of an integrated luminosity of 818 pb^{-1} collected at the $\psi(3770)$ resonance. The upper limit of the decay rate was set to be 9.0×10^{-5} at the 90% confidence level (C.L.) [5]. Since the valence quarks $s\bar{s}$ of the ϕ meson are distinct from those of the D meson ($c\bar{d}$), this process cannot occur in the absence of ω-ϕ mixing or a nonperturbative "weak annihilation" (WA) contribution [6,7]. A measurement of the branching fraction can discriminate which process is dominant. For example, a study of the ratio of $D_s^+ \to \omega e^+\nu_e$ and $D_s^+ \to \phi e^+\nu_e$ [6] concludes that any value of $\mathcal{B}(D_s^+ \to \omega e^+\nu_e)$ exceeding 2×10^{-4} is unlikely to be attributed to ω-ϕ mixing, and would provide evidence for nonperturbative WA effects [7]. A search for the decay $D^+ \to \phi e^+\nu_e$ is helpful, since its dynamics is similar to that of the decay $D_s^+ \to \omega e^+\nu_e$.

We report herein an improved measurement of $\mathcal{B}(D^+ \to \omega e^+\nu_e)$ and the first form factor measurement in this decay. Furthermore, an improved upper limit for $\mathcal{B}(D^+ \to \phi e^+\nu_e)$ is determined. Charge conjugate states are implied throughout this paper. Those decays are studied using a data sample collected with the BESIII detector which corresponds to an integrated luminosity of 2.92 fb^{-1} at the $\psi(3770)$ resonance [8].

The BESIII detector is a spectrometer operating at the BEPCII Collider. The cylindrical core of the BESIII detector consists of a helium-based multilayer drift chamber (MDC), a plastic scintillator time-of-flight system (TOF), and a CsI (Tl) electromagnetic calorimeter (EMC), which are all enclosed in a superconducting solenoid magnet providing a 1.0 T magnetic field. The solenoid is supported by an octagonal flux-return yoke with modules of resistive plate muon counters interleaved with steel. A detailed description of the BESIII detector is provided in Ref. [9].

The tagging technique for the branching fraction measurements of semileptonic decays was first employed by the Mark-III collaboration [10] and later applied in the studies by CLEO-c [4,11]. The presence of a D^+D^- pair in an event allows a *tag sample* to be defined in which a D^- is reconstructed in one of the following six hadronic decay modes: $K^+\pi^-\pi^-$, $K^+\pi^-\pi^-\pi^0$, $K_S^0\pi^-$, $K_S^0\pi^-\pi^0$, $K_S^0\pi^+\pi^-\pi^-$, and $K^+K^-\pi^-$. A subsample is then defined in which a positron and a set of hadrons are required recoiling against

TABLE I. Tag yields in data, tag efficiencies (ϵ_{tag})(%), signal efficiencies including a tag ($\epsilon_{\text{tag,sl}}$)(%) and their statistical uncertainties. All the efficiencies are determined by MC simulations.

Tag mode	N^i_{tag}	ϵ_{tag}	$\epsilon_{\text{tag,sl}}$ (ω)	$\epsilon_{\text{tag,sl}}$ (ϕ)
$K^+\pi^-\pi^-$	809425 ± 906	51.07 ± 0.02	11.22 ± 0.10	9.04 ± 0.09
$K^+\pi^-\pi^-\pi^0$	242406 ± 599	25.13 ± 0.02	5.15 ± 0.09	4.38 ± 0.08
$K^0_S\pi^-$	100149 ± 321	54.40 ± 0.05	11.70 ± 0.32	9.69 ± 0.29
$K^0_S\pi^-\pi^0$	226734 ± 575	29.24 ± 0.02	6.13 ± 0.11	5.34 ± 0.10
$K^0_S\pi^+\pi^-\pi^-$	132683 ± 489	37.61 ± 0.04	7.28 ± 0.18	5.96 ± 0.16
$K^+K^-\pi^-$	70530 ± 325	41.12 ± 0.06	8.97 ± 0.29	7.63 ± 0.27

the tag D meson, as a signature of a semileptonic decay. The absolute branching fraction of the semileptonic decay $\mathcal{B}_{\text{sl}}$ can be expressed as

$$\mathcal{B}_{\text{sl}} = \frac{N_{\text{sig}}}{\sum_i N^i_{\text{tag}} \epsilon^i_{\text{tag,sl}} / \epsilon^i_{\text{tag}}}, \qquad (1)$$

where N_{sig} is the total signal yield in all six tag modes, i indicates a tag mode, N^i_{tag} is the number of observed tag events in mode i, ϵ^i_{tag} is the reconstruction efficiency of mode i, and $\epsilon^i_{\text{tag,sl}}$ is the reconstruction efficiency of the semileptonic decay with tag mode i.

Charged tracks are reconstructed using MDC hit information. The tracks are required to satisfy $|\cos\theta| < 0.93$, where θ is the polar angle with respect to the beam axis. Tracks (except for K^0_S daughters) are required to originate from the interaction point (IP), i.e. their point of closest approach to the interaction point is required to be ± 10 cm along the beam direction and 1 cm transverse to the beam direction. Charged particle identification (PID) is accomplished by combining the dE/dx and TOF information to form a likelihood $\mathcal{L}_i$ ($i = e/\pi/K$) for each particle hypothesis. A $K^\pm$ ($\pi^\pm$) candidate is required to satisfy $\mathcal{L}_K > \mathcal{L}_\pi$ ($\mathcal{L}_\pi > \mathcal{L}_K$). For electrons, we require the track candidate to satisfy $\frac{\mathcal{L}_e}{\mathcal{L}_e + \mathcal{L}_\pi + \mathcal{L}_K} > 0.8$ as well as $E/p \in [0.8, 1.2]$, where E/p is the ratio of the energy deposited in the EMC to the momentum of the track measured in the MDC. To take into account the effect of final state radiation and bremsstrahlung, the energy of neutral clusters within 5° of the initial electron direction is assigned to the electron track. The K^0_S candidates are reconstructed from pairs of oppositely charged tracks, which are assumed to be pions and required to have an invariant mass in the range $m_{\pi^+\pi^-} \in [0.487, 0.511]$ GeV/c^2. For each pair of tracks, a vertex-constrained fit is performed to ensure that they come from a common vertex.

To identify photon candidates, showers must have minimum energies of 25 MeV in the barrel region ($|\cos\theta| < 0.80$) or 50 MeV in the end cap region ($0.86 < |\cos\theta| < 0.92$). To exclude showers from charged particles, a photon candidate must be separated by at least 20° from any charged track with respect to the IP. A requirement on the EMC timing suppresses electronic noise and energy deposits unrelated to the event. The π^0 candidates are reconstructed from pairs of photon candidates by requiring the invariant diphoton mass to fulfill $m_{\gamma\gamma} \in [0.115, 0.150]$ GeV/c^2. Candidates with both photons coming from the end cap region are rejected due to poor resolution.

The D^- tag candidates are selected based on two variables: $\Delta E \equiv E_D - E_{\text{beam}}$, the difference between the energy of the D^- tag candidate (E_D) and the beam energy (E_{beam}), and the beam-constrained mass $M_{\text{bc}} \equiv \sqrt{E^2_{\text{beam}}/c^4 - |\vec{p}_D|^2/c^2}$, where $\vec{p}_D$ is the measured momentum of the D^- candidate. In each event, we accept at most one candidate per tag mode per charge, and the candidate with the smallest $|\Delta E|$ is chosen. The yield of each tag mode is obtained from fits to the M_{bc} distributions [12]. The data sample comprises about 1.6×10^6 reconstructed charged tag candidates (Table I).

Once a D^- tag candidate is identified, we search for an e^+ candidate and an $\omega \to \pi^+\pi^-\pi^0$ candidate or a $\phi \to K^+K^-$ candidate recoiling against the tag. If there are multiple ω candidates in an event, only one combination is chosen based on the proximity of the $\pi^+\pi^-\pi^0$ invariant mass to the nominal ω mass [13]. The invariant mass $m_{\pi^+\pi^-\pi^0} \in [0.700, 0.840]$ GeV/c^2 and $m_{K^+K^-} \in [1.005, 1.040]$ GeV/c^2 are required for ω and ϕ candidates, which correspond to 3 times of the ω (ϕ) mass resolution ($\pm 3\sigma$), respectively. To suppress backgrounds with a K^0_S in the final state, the invariant mass of the charged pions from the $\omega \to \pi^+\pi^-\pi^0$ candidate is required to be outside the aforementioned K^0_S mass region.

After tag and semileptonic candidates have been combined, all charged tracks in an event must be accounted for. The total energy of additional photon candidates, besides those used in the tag and semileptonic candidates, is required to be less than 0.250 GeV. Semileptonic decays are identified using the variable $U \equiv E_{\text{miss}} - c|\vec{p}_{\text{miss}}|$, where E_{miss} and $\vec{p}_{\text{miss}}$ are the missing energy and momentum corresponding to the undetected neutrino from the D^+ meson semileptonic decay, which are calculated by $E_{\text{miss}} \equiv E_{\text{beam}} - E_{\omega(\phi)} - E_e$, $\vec{p}_{\text{miss}} \equiv -(\vec{p}_{\text{tag}} + \vec{p}_{\omega(\phi)} + \vec{p}_e)$ in the center-of-mass frame, where $E_{\omega(\phi)}$ (E_e) and $\vec{p}_{\omega(\phi)}$ ($\vec{p}_e$) are the energy and momentum of the hadron (electron) candidate. To obtain a better U resolution, the momentum of the tag D^- candidate $\vec{p}_{\text{tag}}$ is calculated by $\vec{p}_{\text{tag}} = \hat{p}_{\text{tag}}[(E_{\text{beam}}/c)^2 - M^2_D c^2]^{1/2}$ [14], where $\hat{p}_{\text{tag}}$ is the unit vector in the direction of the tag D^- momentum, and M_D is
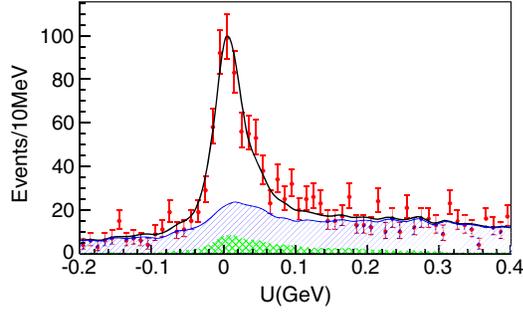
FIG. 1 (color online). Fit (solid line) to the U distribution in data (points with error bars) for the semileptonic decay $D^+ \to \omega e^+ \nu_e$. The total background contribution is shown by the filled curve, while the peaking component is shown by the cross-hatched curve.
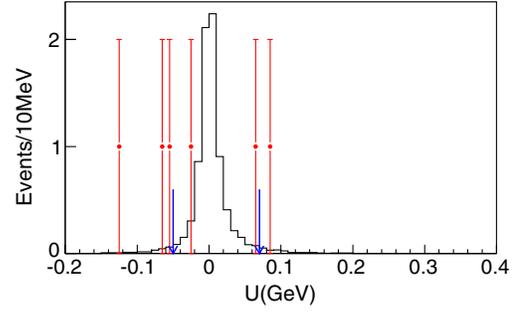

FIG. 2 (color online). The U distribution for the semileptonic decay $D^+ \to \phi e^+ \nu_e$ in data (points with error bars) and signal MC simulation with arbitrary normalization (solid histograms). The arrows show the signal region.

the world average value of D meson mass [13]. The correctly reconstructed semileptonic candidates are expected to peak around zero in the U distribution. A GEANT4-based [15] Monte Carlo (MC) simulation is employed, and events are generated with KKMC + EVTGEN [16,17] to determine the efficiencies in Eq. (1), as shown in Table I. All selection criteria and signal region are defined using simulated events only.

The yield of the decay $D^+ \to \omega e^+ \nu_e$ is obtained from a fit to the U distribution combining all tag modes, as shown in Fig. 1. The signal shape is described by the shape from the signal MC simulation convoluted with a Gaussian function whose width is left free to describe the resolution difference between MC and data. The background model consists of two components: peaking and nonpeaking backgrounds. Peaking background arises mostly from the decay $D^+ \to \bar{K}^{*0} e^+ \nu_e$, $\bar{K}^{*0} \to K_S^0 \pi^0$, $K_S^0 \to \pi^+ \pi^-$; its U distribution is modeled with MC simulation. The largest contribution to the nonpeaking backgrounds is from the $D\bar{D}$ process, while the remaining background events are from the non-$D\bar{D}$, $q\bar{q}$, $\tau^+\tau^-$, initial state radiation $\gamma J/\psi$ and $\gamma\psi(2S)$ processes. The nonpeaking component is modeled with a smooth shape obtained from MC simulations. In the fit to data, the yield of the peaking background is fixed to the MC expectation, while that of the nonpeaking background is left free. The signal yield is determined by the fit to be $N_{sig} = 491 \pm 32$. The absolute branching fraction of the decay $D^+ \to \omega e^+ \nu_e$ as listed in Table II is obtained using Eq. (1).

The U distribution for the decay $D^+ \to \phi e^+ \nu_e$ with all tag modes combined is shown in Fig. 2. The signal region is defined as $[-0.05, 0.07]$ GeV, which covers more than 97% of all signal events. No significant excess of signal events is

observed, and there are only two events in the signal region. A simulation study indicates that the backgrounds arise mostly from $D^+ \to \phi\pi^+\pi^0$ and $D^+ \to \phi\pi^+$ processes. The number of background events is estimated to be 4.2 ± 1.5 via large statistics MC samples. The upper limit is calculated by using a frequentist method with unbounded profile likelihood treatment of systematic uncertainties, which is implemented by a C++ class TROLKE in the ROOT framework [18]. The number of the observed events is assumed to follow a Poisson distribution, and the number of background events and the efficiency are assumed to follow Gaussian distributions. The resulting upper limit on $\mathcal{B}(D^+ \to \phi e^+ \nu_e)$ at 90% C.L. is obtained as listed in Table II.

With the double tag technique, the branching fraction measurements are insensitive to systematics from the tag side since these are mostly canceled. For the signal side, the following sources of systematic uncertainty are taken into account, as summarized in Table III. The uncertainties of tracking and $K^\pm/\pi^\pm$ PID efficiencies are well studied by

TABLE II. Measured branching fractions in this paper and a comparison to the previous measurements [4,5].

Mode	This work	Previous
$\omega e^+ \nu_e$	$(1.63 \pm 0.11 \pm 0.08) \times 10^{-3}$	$(1.82 \pm 0.18 \pm 0.07) \times 10^{-3}$
$\phi e^+ \nu_e$	$< 1.3 \times 10^{-5}$ (90% C.L.)	$< 9.0 \times 10^{-5}$ (90% C.L.)

TABLE III. Summary of systematic uncertainties on the branching fraction measurements.

Source	$\mathcal{B}(D^+ \to \omega e^+ \nu_e)$	$\mathcal{B}(D^+ \to \phi e^+ \nu_e)$
Tracking	3.0%	3.0%
K/π PID	1.0%	1.0%
e PID	3.2%	3.4%
π^0 reconstruction	1.0%	⋯
Model of form factor	1.0%	1.2%
$\omega(\phi)$ decay rate	0.8%	1.0%
MC statistics	0.7%	0.9%
$\omega(\phi)$ mass window	0.9%	0.4%
K_S^0 veto	0.2%	⋯
Extra shower veto	0.1%	0.1%
Signal region	⋯	0.4%
Fit range	0.4%	⋯
Signal shape	0.6%	⋯
Peaking background	0.8%	⋯
Nonpeaking background	0.4%	⋯
Total	5.1%	5.0%

double tagging $D\bar{D}$ hadronic decay events. The uncertainties in $e^{\pm}$ tracking and PID efficiency are estimated with radiative Bhabha events. The uncertainty due to the π^0 reconstruction efficiency is estimated with a control sample $D^0 \to K^-\pi^+\pi^0$ by the missing mass technique. The uncertainty due to imperfect knowledge of the semileptonic form factors is estimated by varying the form factors in the MC simulation according to the uncertainties on the measured form factor ratios in the decay $D^+ \to \omega e^+\nu_e$ as discussed below. For the decay $D^+ \to \phi e^+\nu_e$, the signal MC produces phase-space distributed events, and therefore uses a constant form factor. To evaluate the corresponding systematics, the form factor is varied by a reweighting technique [19]. The world average values of $\mathcal{B}(\omega \to \pi^+\pi^-\pi^0)$ and $\mathcal{B}(\phi \to K^+K^-)$ are $(89.2 \pm 0.7)\%$ and $(48.9 \pm 0.5)\%$, respectively, and their uncertainties are assigned as systematic uncertainties due to the input branching fractions in the MC simulation. The limited MC statistics also leads to a systematic uncertainty. The uncertainties associated with the ω or ϕ mass requirements are estimated using the control samples $D^0 \to \omega K^-\pi^+$ and $D^+ \to \phi\pi^+$, respectively. The K^0_S rejection leads to an uncertainty on the signal efficiency of the decay $D^+ \to \omega e^+\nu_e$, which is studied by the control sample $D^0 \to \omega K^-\pi^+$. The uncertainty due to the extra shower veto is studied with double hadronic tags. For the decay $D^+ \to \phi e^+\nu_e$, the uncertainty due to the signal region requirement is estimated by the control sample

$D^+ \to \bar{K}^{*0}e^+\nu_e$, $\bar{K}^{*0} \to K^-\pi^+$. In the fit to the U distribution in the $D^+ \to \omega e^+\nu_e$ decay, the uncertainty due to the parametrization of the signal shape is estimated by varying the signal shape to a Crystal Ball function [20]. The uncertainty due to the fit range is estimated by varying the fit range. The uncertainty due to the nonpeaking background is estimated by modeling this component with a third-order Chebychev function, and the uncertainty associated with the fixed peaking background normalization is estimated by varying it within its expected uncertainty. All of those estimates are added in quadrature to obtain the total systematic uncertainties on the branching fractions.

The differential decay rate of $D^+ \to \omega e^+\nu_e$ can be expressed in the following variables as illustrated in Fig. 3: m^2, the mass square of the $\pi\pi\pi$ system; q^2, the mass square of the $e\nu_e$ system; θ_1, the ω helicity angle [21], which is the angle between the ω decay plane normal ($\hat{n}$) in the $\pi\pi\pi$ rest frame and the direction of flight of the ω in the D rest frame; θ_2, the helicity angle of e, which is the angle between the charged lepton three-momentum in the $e\nu_e$ rest frame and the direction of flight of the $e\nu_e$ system in the D rest frame; χ, the angle between the decay planes of those two systems.

For the differential partial decay width, only the P-wave component is taken into consideration and the formalism expressed in terms of three helicity amplitudes $H_+(q^2)$, $H_-(q^2)$, and $H_0(q^2)$ is [4,22,23]

$$
\begin{aligned}
\frac{d\Gamma}{dq^2 d\cos\theta_1 d\cos\theta_2 d\chi dm_{\pi\pi\pi}} = {} & \frac{3}{8(4\pi)^4}G_F^2|V_{cd}|^2\frac{p_\omega q^2}{M_D^2}\mathcal{B}(\omega \to \pi\pi\pi)|\mathcal{BW}(m_{\pi\pi\pi})|^2[(1+\cos\theta_2)^2\sin^2\theta_1|H_+(q^2,m_{\pi\pi\pi})|^2 \\
& + (1-\cos\theta_2)^2\sin^2\theta_1|H_-(q^2,m_{\pi\pi\pi})|^2 + 4\sin^2\theta_2\cos^2\theta_1|H_0(q^2,m_{\pi\pi\pi})|^2 \\
& + 4\sin\theta_2(1+\cos\theta_2)\sin\theta_1\cos\theta_1\cos\chi H_+(q^2,m_{\pi\pi\pi})H_0(q^2,m_{\pi\pi\pi}) \\
& - 4\sin\theta_2(1-\cos\theta_2)\sin\theta_1\cos\theta_1\cos\chi H_-(q^2,m_{\pi\pi\pi})H_0(q^2,m_{\pi\pi\pi}) \\
& - 2\sin^2\theta_2\sin^2\theta_1\cos 2\chi H_+(q^2,m_{\pi\pi\pi})H_-(q^2,m_{\pi\pi\pi})],
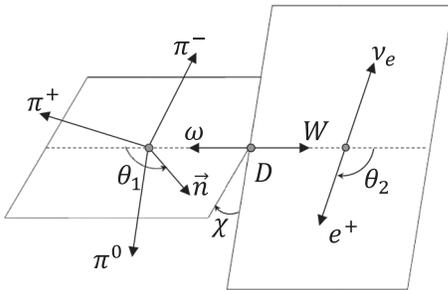\end{aligned}
\tag{2}
$$

FIG. 3. Definitions of the helicity angles in the decay $D^+ \to \omega W^+$, $\omega \to \pi^+\pi^-\pi^0$, $W^+ \to e^+\nu_e$ for the three-body (θ_1) and two-body (θ_2) D^+-daughter decays, where both angles are defined in the rest frame of the decaying meson.

where G_F is the Fermi constant, p_ω is the ω momentum in the D rest frame, $\mathcal{B}(\omega \to \pi\pi\pi)$ is the branching fraction of $\omega \to \pi\pi\pi$, $m_{\pi\pi\pi}$ is the invariant mass of the three pions, and $\mathcal{BW}(m_{\pi\pi\pi})$ is the Breit-Wigner function that describes the ω line shape. The helicity amplitudes can in turn be related to the two axial-vector form factors $A_{1,2}(q^2)$ and the vector form factor $V(q^2)$. For the q^2 dependence, a single pole parametrization [24] is applied:

$$
V(q^2) = \frac{V(0)}{1-q^2/m_V^2}, \qquad A_{1,2}(q^2) = \frac{A_{1,2}(0)}{1-q^2/m_A^2}, \tag{3}
$$

where the pole masses m_V and m_A are expected to be close to $M_{D^*(1^-)} = 2.01$ GeV/c^2 and $M_{D^*(1^+)} = 2.42$ GeV/c^2 [13] for the vector and axial form factors, respectively. The ratios of these form factors, evaluated at $q^2 = 0$, $r_V = \frac{V(0)}{A_1(0)}$ and $r_2 = \frac{A_2(0)}{A_1(0)}$, are measured in this paper.
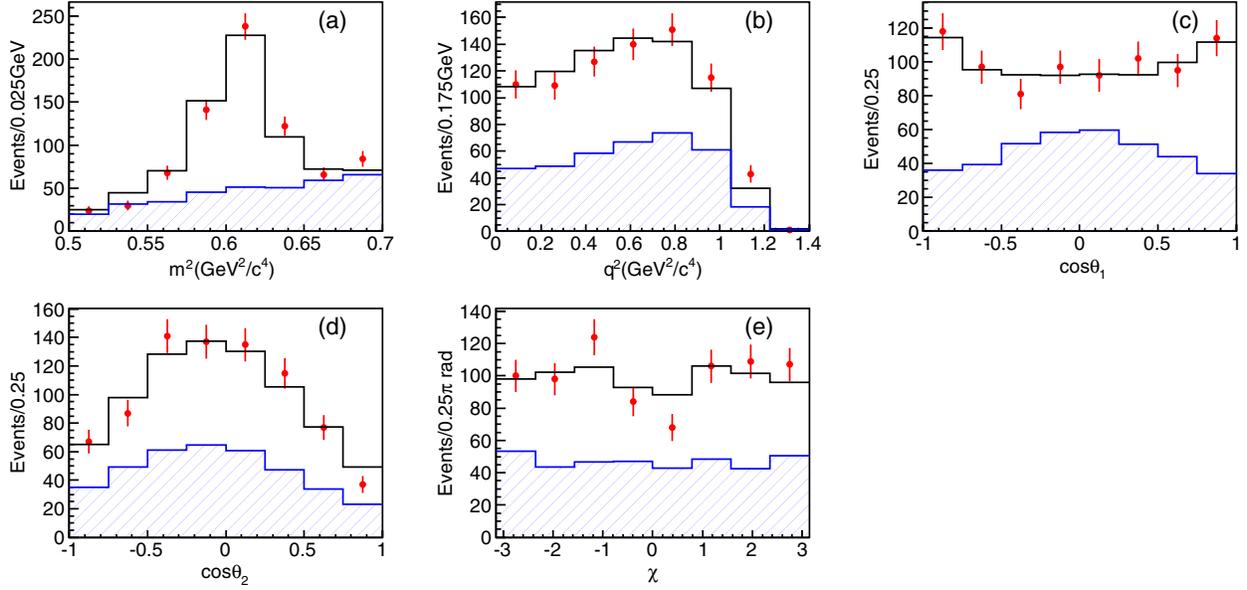
FIG. 4 (color online). Projections of the data set (points with error bars), the fit results (solid histograms) and the sum of the background distributions (filled histogram curves) onto (a) m^2, (b) q^2, (c) $\cos\theta_1$, (d) $\cos\theta_2$ and (e) χ.

According to the fit procedure introduced in Ref. [3], a five-dimensional maximum likelihood fit is performed in the space of m^2, q^2, $\cos\theta_1$, $\cos\theta_2$ and χ. The signal probability density function is modeled with the phase-space signal MC events reweighted with the decay rate [Eq. (2)] in an iterative procedure. Large signal MC samples are generated to reduce the systematic uncertainty associated with the MC statistics. The background is modeled with the MC simulation and its normalization is fixed to the expectation. Using simulated events with known r_V and r_A, we verify that this procedure can reliably determine the form factor ratios. Figure 4 shows the m^2, q^2, $\cos\theta_1$, $\cos\theta_2$ and χ projections from the final fit to data. The fit determines the form factor ratios to be $r_V = 1.24 \pm 0.09$ and $r_2 = 1.06 \pm 0.15$.

For this form factor measurement, the following sources of systematic uncertainties are taken into account, and the estimate of their magnitude are given in parentheses for r_V and r_2, respectively. The uncertainty associated with the unknown q^2 dependence of the form factors (0.05, 0.03) is estimated by introducing a double pole parametrization [25]. The uncertainty due to the background model (0.02, 0.02) is estimated by varying the background normalization with its statistical uncertainty. No events from the non-resonant decay $D^+ \to \pi^+\pi^-\pi^0 e^+\nu_e$ are observed, the influence of this decay on the form factor therefore can be neglected. To estimate the uncertainty associated with the pole mass assumption (0.01, negligible), we vary the pole mass m_V by ± 100 MeV/c^2 and find the change on r_2 is so small that it can be neglected. A small shift is observed with the presence of background (0.02, 0.02), and this is treated as a possible bias in the form factor fitting procedure. Adding all systematic uncertainties in

quadrature, the form factor ratios are determined to be $r_V = 1.24 \pm 0.09 \pm 0.06$ and $r_2 = 1.06 \pm 0.15 \pm 0.05$, respectively.

In summary, using 2.92 fb^{-1} of e^+e^- annihilation data collected at the $\psi(3770)$ resonance, we have measured the form factor ratios in the decay $D^+ \to \omega e^+\nu_e$ at $q^2 = 0$ for the first time: $r_V = \frac{V(0)}{A_1(0)} = 1.24 \pm 0.09 \pm 0.06$, $r_2 = \frac{A_2(0)}{A_1(0)} = 1.06 \pm 0.15 \pm 0.05$, and determined the branching fraction to be $\mathcal{B}(D^+ \to \omega e^+\nu_e) = (1.63 \pm 0.11 \pm 0.08) \times 10^{-3}$, where the first and the second uncertainties are statistical and systematic, respectively. This is the most precise measurement to date. We have also searched for the rare decay $D^+ \to \phi e^+\nu_e$ and observe no significant signal. We set an upper limit of $\mathcal{B}(D^+ \to \phi e^+\nu_e) < 1.3 \times 10^{-5}$ at the 90% C.L., which improves the upper limit previously obtained by the CLEO Collaboration [5] by a factor of about 7.

---

[1] N. Cabibbo, Unitary Symmetry and Leptonic Decays, Phys. Rev. Lett. **10**, 531 (1963).

[2] M. Kobayashi and T. Maskawa, CP violation in the renormalizable theory of weak interaction, Prog. Theor. Phys. **49**, 652 (1973).

[3] P. del Amo Sanchez *et al.* (*BABAR* Collaboration), Analysis of the $D^+ \to K^- \pi^+ e^+ \nu_e$ decay channel, Phys. Rev. D **83**, 072001 (2011).

[4] S. Dobbs *et al.* (CLEO Collaboration), First Measurement of the Form Factors in the Decays $D^0 \to \rho^- e^+ \nu_e$ and $D^+ \to \rho^0 e^+ \nu_e$, Phys. Rev. Lett. **110**, 131802 (2013).

[5] J. Yelton *et al.* (CLEO Collaboration), Studies of $D^+ \to \eta', \eta, \phi e^+ \nu_e$, Phys. Rev. D **84**, 032001 (2011).

[6] M. Gronau and J. L. Rosner, omega-phi mixing and weak annihilation in D(s) decays, Phys. Rev. D **79**, 074006 (2009).

[7] I. I. Bigi and N. G. Uraltsev, Weak annihilation and the end-point spectrum in semileptonic B decays, Nucl. Phys. **B423**, 33 (1994); H. Y. Cheng, Weak annihilation and the effective parameters a_1 and a_2 in non-leptonic D decays, Eur. Phys. J. C **26**, 551 (2003).

[8] M. Ablikim *et al.* (BESIII Collaboration), Measurement of the integrated luminosities of the data taken by BESIII at $\sqrt{s} = 3.650$ and 3.773 GeV, Chin. Phys. C **37**, 123001 (2013).

[9] M. Ablikim *et al.* (BESIII Collaboration), Design and construction of the BESIII detector, Nucl. Instrum. Methods Phys. Res., Sect. A **614**, 345 (2010).

[10] J. Adler *et al.* (MARK-III Collaboration), Measurement of the Branching Fractions for $D^0 \to \pi^- e^+ \nu_e$ Electron-Neutrino and $D^0 \to K^- e^+ \nu_e$ Electron-Neutrino and Determination of $\|V_{cd}/V_{cs}\|^2$, Phys. Rev. Lett. **62**, 1821 (1989).

[11] G. S. Huang *et al.* (CLEO Collaboration), Absolute Branching Fraction Measurements of Exclusive D^+ Semileptonic Decays, Phys. Rev. Lett. **95**, 181801 (2005).

[12] M. Ablikim *et al.* (BESIII Collaboration), Precision measurements of $B(D^+ \to \mu^+ \nu_\mu)$, the pseudoscalar decay constant f_{D^+}, and the quark mixing matrix element $|V_{cd}|$, Phys. Rev. D **89**, 051104 (2014).

[13] K. A. Olive *et al.* (Particle Data Group), Review of particle physics, Chin. Phys. C **38**, 090001 (2014).

[14] T. E. Coan *et al.* (CLEO Collaboration), Absolute Branching Fraction Measurements of Exclusive D^0 Semileptonic Decays, Phys. Rev. Lett. **95**, 181802 (2005).

[15] S. Agostinelli *et al.* (GEANT4 Collaboration), GEANT4: A simulation toolkit, Nucl. Instrum. Methods Phys. Res., Sect. A **506**, 250 (2003).

[16] S. Jadach, B. F. L. Ward, and Z. Was, The precision Monte Carlo event generator κκ for two-fermion final states in $e^+ e^-$ collisions, Comput. Phys. Commun. **130**, 260 (2000); Coherent exclusive exponentiation for precision Monte Carlo calculations, Phys. Rev. D **63**, 113009 (2001).

[17] D. J. Lange, The EvtGen particle decay simulation package, Nucl. Instrum. Methods Phys. Res., Sect. A **462**, 152 (2001).

[18] W. A. Rolke, A. M. Lopez, and J. Conrad, Limits and confidence intervals in the presence of nuisance parameters, Nucl. Instrum. Methods Phys. Res., Sect. A **551**, 493 (2005).

[19] L. Martin *et al.* (CLEO Collaboration), Search for the decay $D_s^+ \to \omega e^+ \nu$, Phys. Rev. D **84**, 012005 (2011).

[20] J. Gaiser, Ph. D. thesis, Stanford University [Report No. SLAC-255, 1982]; T. Skwarnicki, Ph. D. thesis, Jagiellonian University in Krakow [DESY Report No. F31-86-02, 1986].

[21] S. M. Berman and M. Jacob, Systematics of angular and polarization distributions in Three-Body decays, Phys. Rev. **139**, B1023 (1965).

[22] J. G. Korner and G. A. Schuler, Exclusive semileptonic heavy meson decays including lepton mass effects, Z. Phys. C **46**, 93 (1990).

[23] F. J. Gilman and R. L. Singleton, Analysis of semileptonic decays of mesons containing heavy quarks, Phys. Rev. D **41**, 142 (1990).

[24] J. D. Richman and P. R. Burchat, Leptonic and semileptonic decays of charm and bottom hadrons, Rev. Mod. Phys. **67**, 893 (1995).

[25] S. Fajfer and J. F. Kamenik, Charm meson resonances and $D \to V$ semileptonic form factors, Phys. Rev. D **72**, 034029 (2005).